Turboboosting Visible Light Backscatter Communication

Yue Wu, Purui Wang, Kenuo Xu, Lilei Feng, Chenren Xu*

Peking University

ABSTRACT

Visible light backscatter communication (VLBC) presents an emerging low power IoT connectivity solution with spatial reuse and interference immunity advantages over RF-based (backscatter) technologies. State-of-the-art VLBC systems employ COTS LCD shutter as optical modulator, whose slow response fundamentally throttles its data rate to sub-Kbps, and limits its deployment at scale for use cases where higher rate and/or low latency is a necessity.

We design and implement RetroTurbo, a VLBC system dedicated for turboboosting data rate. At the heart of RetroTurbo design is a pair of novel modulation schemes, namely delayed superimposition modulation (DSM) and polarization-based QAM (PQAM), to push the rate limit by strategically coordinating the state of a liquid crystal modulator (LCM) pixel array in time and polarization domains. Specifically, DSM ensures we fully exploit the available SNR for high order modulation in the LCM-imposed nonlinear channel; PQAM is based on polarized light communication that creates a QAM design in polarization domain with flexible angular misalignment between two ends. A real-time near-optimal demodulation algorithm is designed to ensure system's robustness to heterogeneous signal distortion. Based on our prototyped system, RetroTurbo demonstrates 32x and 128x rate gain via experiments and emulation respectively in practical real-world indoor setting.

CCS CONCEPTS

• **Hardware → Wireless devices**; • **Computer systems organization →** *Embedded systems.*

KEYWORDS

Visible Light Backscatter Communication; Delayed Superimposed Modulation; Polarization-based QAM

ACM Reference Format:

Yue Wu, Purui Wang, Kenuo Xu, Lilei Feng, Chenren Xu. 2020. Turboboosting Visible Light Backscatter Communication. In *Annual conference of the ACM Special Interest Group on Data Communication on the applications, technologies, architectures, and protocols for computer communication (SIGCOMM '20), August 10–14, 2020, Virtual Event, NY, USA.* ACM, New York, NY, USA, 12 pages. https://doi.org/10.1145/3387514.3406229

*Y.Wu and P.Wang are the co-primary student authors.

✉: chenren@pku.edu.cn

SIGCOMM '20, August 10–14, 2020, Virtual Event, NY, USA

ACM ISBN 978-1-4503-7955-7/20/08…$15.00

https://doi.org/10.1145/3387514.3406229

1 INTRODUCTION

As the Internet of Things (IoT) is turning into reality at a quick pace, billions or even trillions of ambient objects are expected to gain Internet access in the near future to benefit everyday life. However, such massive scaling poses grand challenges of energy management in real-world deployment – today's wireless technology for IoT (*e.g.,* BLE, WiFi, ZigBee, Lora, and NB-IoT) typically operates at tens or hundreds of milliwatt, which is a mismatch with long-term deployment without battery replacements. In other words, a much lower power wireless communication (and networking) solution is highly desirable to realize the IoT vision at scale truly.

Recently, backscatter communication has become an active research front, as it effectively offers merely orders of μW connectivity to small sensors and hereby becomes a compelling communication solution candidate in the IoT era. Essentially, backscatter communication suppresses energy consumption by reflection rather than transmission – most recent work even shows it is possible to hitchhike the information over the ambient signals such as WiFi [1–4], FM [5] and Lora [6, 7] radio to further improve its deployability. However, radio backscatter will bring two potential issues when deployed for indoor IoT scenarios: *i*) it interferes with normal daily traffic, and exacerbates the "spectrum crunch" problem; *ii*) its leakage through wall yields serious security and privacy concerns in room-area networking use cases [8] where adhering to physical room boundaries is an essential requirement.

Along the line but exploring a different medium, visible light backscatter communication (VLBC) [9–11] presents an emerging and potentially better solution. First, optical medium intrinsically addresses the RF interference, security and privacy problems aforementioned in room-level networking. Second, based on the idea of modulating retroreflection with a LCD shutter (or liquid crystal modulator, LCM in essence), a low cost passive optical transmitter together with the retroreflective uplink design is built dedicated for power-constrained ends and reliable bidirectional communication with high spatial-spectral efficiency. However, LCM, the key component to realize modulation, also becomes the bottleneck – its low refreshing/switch rate (*i.e.,* 100 – 240 Hz) fundamentally limits the data rate. PassiveVLC [9] achieves the highest rate ever by pushing the limit of symbol length for slope detection, which is still no more than 1 Kbps. Considering an embedded VLC (down)link can easily achieve more than tens or even hundreds of Kbps [12], a slow (*i.e.,* sub-Kbps) uplink can easily become the bottleneck in a duplex link, and the situation is even worse in a networked environment. From the channel capacity perspective, our key insight is that due to the nonlinearity resulting from LCM-based modulation, the available channel capacity is not fully utilized when the link has a sufficiently high SNR, *i.e.,* the SNR is not efficiently traded off for data rate. Hence, we ask the following question: *How can we fully exploit the channel capacity, and/or even explore more independent channels to boost the data rate in VLBC?*

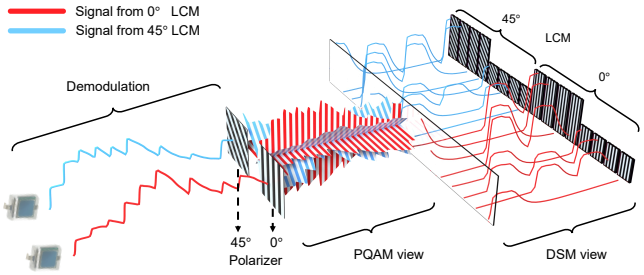

Figure 1: Illustration of RetroTurbo modulation process with 4-order DSM and 4-order PQAM.

To answer the first part of the question, our key observation is that the pulse response of LCM is highly asymmetric: charging is much faster than discharging, *e.g.,* sub-ms versus 4 ms. By strategically interleaving the charging and discharging state on each LCM pixel, we present a Delayed Superimposed Modulation (DSM) scheme that modulates information with the superimposed LCMs' pulse response. In this way, DSM leads to a inter-symbol interference (ISI) channel, provides approximately linear capacity gain to the resolution of LCM pixel array, and fully utilizes the available bandwidth on this unconventional nonlinear optical channel.

To further explore additional channels to increase overall link capacity, we propose a polarization-based quadrature amplitude modulation (PQAM) that fully utilizes two orthogonal polarization channels. The design of PQAM is inspired by polarization division multiplexing (PDM) [13] and QAM, but fundamentally different from their combinations in that it constructs the orthogonal basis in the polarization domain rather than the phase domain by exploiting the polarization manipulation capability of LCM. Most importantly, unlike PDM, PQAM will not sacrifice rate when (polarity) angular misalignment happens – instead, it always provides full rate with an arbitrary relative orientation between two ends, which is essential for facilitating IoT deployment in the wild.

The generated signal waveform from each LCM pixel (with different size and polarization angle) and their DSM-PQAM synthesis process is illustrated in Fig. 1. The retroreflected carrier light signals are first polarized (again) into two different angles (*i.e.,* 0° and 45°) and allocated to the corresponding PQAM channels, and then OOK-modulated in a interleaving manner for DSM symbol construction in each PQAM channel for further demodulation. The demodulation process actually poses several practical challenges to be addressed. First, the ISI channel resulting from DSM introduces nonlinearity from the unique characteristics of LCM, which cannot be solved by conventional nonlinear equalizer efficiently. Second, the LCMs' pulse response will experience diverse signal distortion introduced by different previous channel state, relative location and incidence angle towards light sensor. We design a multi-branch decision-feedback equalizer and a online-offline channel training algorithm not only address all the demodulation challenges aforementioned, but also provide real-time near-optimal performance. Note that we only need two photodiodes rather than a camera-like large pixel array for DSM-PQAM signal demodulation.

We implemented a prototype system called RetroTurbo based on the DSM and PQAM designs. Our experimental results show RetroTurbo can achieve as high as 8 Kbps with a communication range up to 7.5 m under a sub-mW power budget, and the link is reliable in various indoor IoT settings, including different relative angular misalignment, ambient light and human mobility. Our trace-driven emulation further showcases the RetroTurbo's advanced modulation scheme design can support up to 32 Kbps, and achieve as high as 3.7x aggregated throughput gain with a link-aware rate-adaptive MAC protocol in networked environment.

Contributions.

- We propose a pair of novel modulation schemes namely DSM (§4.1) and PQAM (§4.2) to explore and fully utilize the channel capacity in both time and polarization domains to push rate limit of practical visible light backscatter communication.
- We design a demodulation algorithm incorporated with decision feedback equalizer and online-offline channel training to ensure real-time near-optimal performance in the presence of heterogeneous signal distortion (§4.3).
- We provide a general modulation scheme analysis method for demodulation threshold estimation on nonlinear modulator and optimal parameter determination for DSM and PQAM under different channel conditions (§5).
- We build a RetroTurbo prototype system (§6) that demonstrates 32x and 128x data rate over the OOK baseline in experimental and emulation results (§7).

Finally, we acknowledge that the highest rate of 8 Kbps supported by our prototype (and even 32 Kbps by emulation) is two or three order slower than status-quo multi-Mbps radio backscatter system. We would like to note that the RetroTurbo design can be easily applied on much faster switching liquid crystal (*e.g.,* CCN-47 with 30 ns [14] and ferroelectric with 20 µs [15] restoration time) that has become technically viable. We envision an integrated solution will catch up this cap and provide better performance soon.

2 BACKGROUND

2.1 Visible Light Backscatter Communication

Visible light backscatter communication (VLBC) aims to enable uplink operation from low power tags to lighting infrastructure or readers (in analogy to RFID system) via modulated optical reflection over the visible light communication medium. The status-quo VLBC schemes exploit retroreflective fabric to direct the reflected light beam towards the (interrogating) reader, and toggle on/off states of an COTS LCD shutter to modulate the reflected light carrier via trend-based on-off keying (OOK) [9] – the "on" and "off" state of OOK realized by LCD as an optical modulator (§2.2) is modulated as decreasing or increasing trend due to its ms-level low state transition time rather than a high and low pulse. Another approach is to borrow the idea of pulse amplitude modulation (PAM) by using multiple LCD pixels [10]. Specifically, it's composed of pixels whose area is $1{:}2{:}\cdots{:}2^M$, and selectively turn on or off each pixel to realize M-order modulation, *i.e.,* carry M-bit information per symbol. PAM improves spectral efficiency over OOK in that it utilizes the amplitude resolution when SNR is sufficiently high, but still is fundamentally limited by LCD's slow refreshing rate. The slow rate also introduces the flickering issue to both schemes to potentially impair people's inclination to make use of such techniques, which can be solved by polarized light communication [11].

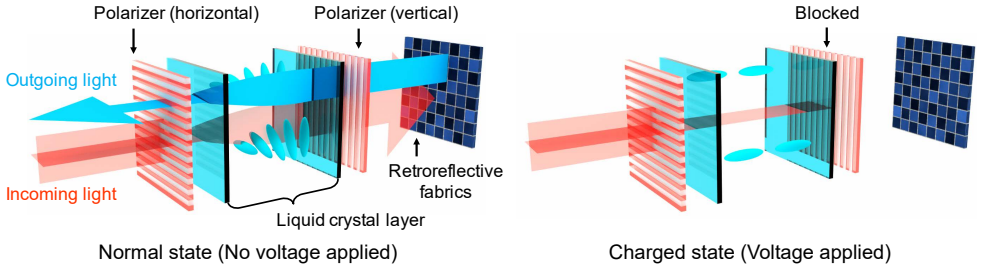

Figure 2: Principle of LCD-based VLBC.

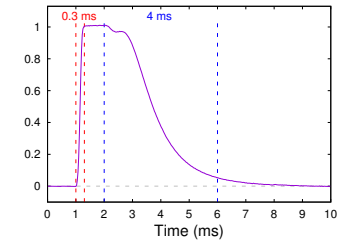

Figure 3: Asymmetric edges in LCD pulse response.

2.2 LCD as Optical Modulator

LCD shutter is a device with multi-layer sandwich structure that has two polarizer films with orthogonal polarization direction at two ends and an in-middle liquid crystal layer. A polarizer will polarize the incoming light to its polarization direction. In the natural state the liquid crystal rotates the light polarity by 90° because of the intermolecular force, and keeps the original light polarity with electric force when it is being charged – this underlying mechanism determines that it cannot rotates light polarity by an arbitrary angle. Fig. 2 illustrates how to realize OOK-based VLBC with LCD shutter as optical modulator. For instance, when LCD is in its normal (uncharged) state, the horizontally polarized incoming light (after passing the front polarizer) will become vertically polarized after passing the liquid crystal so then it is able to pass the back polarizer (twice), and eventually pass the front polarizer for the second time after another optical rotation of 90°.

By taking a closer look at the response curve for LCD's charging state transition, we found it highly asymmetric – charging phase can be finished within 0.3 ms, while the discharging phase lasts as long as 4 ms (Fig. 3)[1]. Specifically, we observe a ~1 ms relatively flat pulse in the beginning of discharging phase due to the intrinsic properties of the liquid crystal. Evidently, LCD as a nonlinear transmitter [16] poses challenges in modulation and modeling.

Note that for LCD, the key to realize optical modulation is to manipulate light polarization with the electric-controlled liquid crystal layer. Given that the RetroTurbo design leverages a modified LCD with its front polarizer detached, we call it *liquid crystal modulator (LCM)* in the rest of the paper.

3 RETROTURBO OVERVIEW

3.1 Design Goals

High Bandwidth Utilization. The modulation scheme design should fully utilize the available channel and link capacity and SNR to boost the data rate as high as possible.

Flexible Orientation. As the relative orientation between two ends can be arbitrary in real-world deployment, the preamble design should provide link performance with high fidelity regardless of the angular misalignment.

Scalability. Higher order symbol construction and the consequent higher data rate come from more LCM pixels, which also invites increasing level of channel response complexities from the heterogeneity in previous channel state, illumination condition and manufacturing process of each pixel. The demodulation design should tolerate such system error.

[1]The two values shown in this example do not mean to the actual time duration for the LCD to be *fully* charged and discharged respectively.

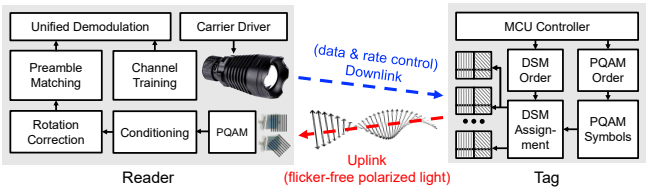

Figure 4: RetroTurbo Architecture.

3.2 System Overview

RetroTurbo is a high rate, flexible orientation and scalable VLBC PHY design, and focuses on the tag-to-reader link (Fig. 4). At a high level, the reader emits unpolarized light as the excitation carrier, which will be reflected by the retroreflector substrate on the tag side, and further manipulated in both time and polarization domain with an LCM pixel array for data transmission.

Tag. It is composed of a backscatter controller and an array of LCM pixels with retroreflector substrate as an optical antenna. The controller determines a modulation scheme based on link protocol or explicit information from downlink, and toggles each individual LCM pixel accordingly for operation. The LCM array has two groups of pixels of different size with polarization angle of 0° or 45°. Each group generates a DSM symbol (§4.1) by fully utilizing the SNR of a single channel, and the two groups collaboratively realize PQAM on two orthogonal polarization channels for flicker-free and additional bandwidth exploitation purposes (§4.2).

Reader. The modulated retroreflected signal in arbitrary angle is first passed to a real-time preamble detector that synchronizes time and corrects the angular rotation (§4.3.1). Then the demodulation process is based on decision-feedback equalizer (§4.3.2) that balances its error-performance and computational cost, as well as channel training (§4.3.3) for accurate channel estimation in the presence of LCM pixel heterogeneity to ensure scalability.

MAC. RetroTurbo also incorporates a simple MAC layer that features the link-aware rate adaptation functionality for performance and reliability enhancement.

4 RETROTURBO DESIGN

This section presents two complementary advanced modulation schemes and their unified demodulation algorithm to achieve tens of times rate gain over the status quo, as well as a simple MAC protocol for rate adaptation. Tab. 1 summarizes the symbols used in RetroTurbo design and their typical value.

Symbol	Parameter Definition	Typical Value
τ_1	Charging phase duration	0.5 ms
τ_0	Discharging phase duration	3.5 ms
L	DSM order	8
T	DSM interleaving time	0.5 ms
W	DSM symbol duration ($= L \times T = \tau_1 + \tau_0$)	4 ms
P	PQAM order	16
V	Tail effect in DSM symbols	2

Table 1: Parameters in RetroTurbo design.

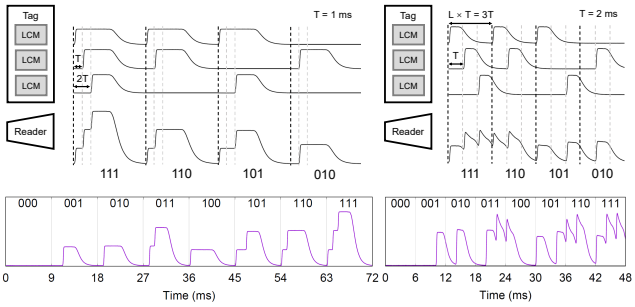

(b) DSM.

Figure 5: Illustration of 3-order DSM.

4.1 Delayed Superimposition Modulation

4.1.1 *Basic Design*

The design of DSM is based on the observation that the response time of LCM's state transition is highly asymmetric, *i.e.,* the fast edge or charging phase of τ_1 can be several times faster than the slow edge or discharging phase of τ_0[2] – this property essentially makes the slow edge the performance bottleneck in status-quo VLBC modulation schemes like OOK and PAM. In addition, LCM's pulse response is neither linear [16] nor sinusoid (Fig. 3), which leaves great challenges in manipulating amplitude, frequency and phase, *i.e.,* it is very difficult to apply or even design advanced modulation scheme in RF domain that can trade off SNR for higher data rate. However, despite the challenges that a single LCM's pulse response is nonlinear to the driving signal, multiple LCM's responses will be linearly superimposed in reception.

Following this simple intuition, our basic idea is to utilize the fast edges from multiple LCM pixels exclusively for modulation, which in essence leverages their constructed temporal diversity. Specifically, we interleave the time slot τ_1 of the charging phase on different LCM pixels, and selectively fire each of them to construct different waveforms or DSM symbols to realize L-order basic DSM, where L is the number of LCM response with different timing to fire in each symbol. As an example of 3-order basic DSM shown in Fig. 5a, there are three fast edges in three different time slots interleaved by T contributed by three individual LCM pixels. They each represent a single bit and together form a basic DSM symbol carrying 3-bit information. We set T to be at least τ_1, *e.g.,* 1 ms, to avoid overlapping fast edges and thus balance the SNR requirement and modulation efficiency. Note that a slow edge of τ_0 is necessary for every single LCM pixel to return to the discharged state before switching back to the charged state for modulation, and therefore it takes τ_0 following the latest fast edge to wrap up a basic DSM symbol. This is because failing to satisfy the timing constraints of fully discharging will lead to inter-symbol interference (ISI) when LCM is not switched back to its stable (*i.e.,* fully discharged) state before the next symbol starts, and consequently higher SNR requirement due to less received energy per bit.

The highest data rate that can be achieved is constrained by how fast the charging phase can ramp up. The L-th order basic DSM has a symbol length of $L \times \tau_1 + \tau_0$, and thus the overall data rate of DSM is: $L/(L \times \tau_1 + \tau_0)$. Note that DSM is specially designed for asymmetric state transitions. Unlike OOK and PAM, the slower edge is no longer the bottleneck when L is sufficiently large so that rate converges to $1/\tau_1$. However, a small L (*e.g.,* less than τ_0/τ_1) is often selected to balance data rate and $1/L$ signal strength per bit given the limited area of LCM in practice. Therefore, it is worth exploring how to improve the basic DSM design to reduce the overhead of τ_0 while keeping L small.

[2]The typical value of τ_1 and τ_0 are empirically chosen to balance the modulation efficiency and SNR. Specifically, τ_0 of 3.5 ms is chosen for higher data rate while introducing tail effect to be discussed in §4.3.3.

4.1.2 *Make DSM even Faster*

To reiterate, the inefficiency of basic DSM design, *i.e.,* the overhead of τ_0, comes from the fact that one LCM pixel has to wait for others before starting to discharge. However, the firstly-fired LCM pixel could have started to discharge as soon as it finishes the charging phase. Based on this idea, we have all the L LCMs generate the same pulse response interleaved by time T, during which each LCM pixel stays in charging state. The new DSM symbol of order L has a length W of LT, composed of L overlapped LCMs' response. We show an example of $T = 2$ ms in Fig. 5b. The pulse response of a single LCM is defined as $p(t)$ which has zero value when $t < 0$ or $t >= W$. Given the noise signal $n(t)$ and transmit bit sequence I_n, the received waveform is:

$$r(t) = n(t) + \sum_n I_n p(t - nT),$$

so that at most L bits ISI is introduced. The highest rate of DSM is $1/\tau_1$ when $T = \tau_1$, essentially eliminating the constraint of τ_0. Similar to basic DSM, L contributes the demodulation threshold. We defer the discussion on L optimization in §5.3.

We would like to note that the DSM design is essentially a partial response signaling (PRS) scheme based on the philosophy to improve bandwidth utilization with L overlapped modulators at the cost of ISI that spans L symbols. PRS works by keeping the ISI into deterministic and controlled ones, which could be reverted to a non-ISI channel for modeling and estimation. However, conventional PRS systems [17] focus on linear transmitters to shape the system spectrum, to which LCM is not applied due to its nonlinearity. DSM is different from AM in that it is a digital modulation scheme – it constructs the modulation symbols with finite amplitudes from pulse response generated by multi-pixel LCM. In addition, among the solutions to ISI channel in general, our DSM approach requires least modification to the transmitter but requires the ISI pattern to be a known constant. This is because the exhibited nonlinearity of LCM makes it very difficult to manipulate it to an arbitrary level of opacity quickly and maintain a predictable transitory response

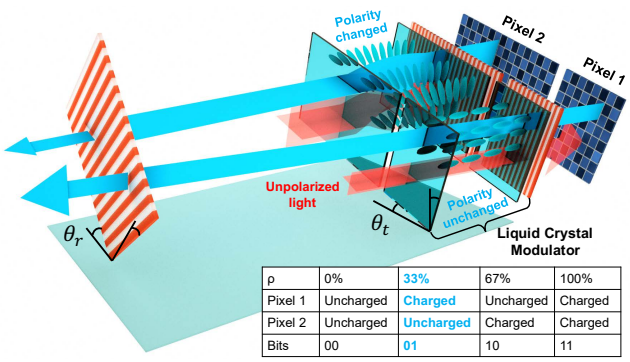

ρ	0%	33%	67%	100%
Pixel 1	Uncharged	Charged	Uncharged	Charged
Pixel 2	Uncharged	Uncharged	Charged	Charged
Bits	00	01	10	11

Figure 6: Illustration of 4-PAM in polarized light communication with angular misalignment on two ends.

at the same time, both of which are a structured pre-equalization-based ISI solution, say, OFDM, would demand. On the other hand, the structure and transmitter complexity of OFDM is the cost for receiver's easy estimation of unknown and diverged ISI response as the per-subcarrier CSI, which is also unnecessary as the LCM's ISI pattern is stable and repeatable, and can be characterized with a few parameters (§4.3.3) after an offline training.

4.2 Polarization-based QAM

While the DSM design makes a decent effort on pushing the rate limit on a single channel, it is always beneficial to explore additional independent channels for more link bandwidth. We propose to exploit polarization-based channel diversity because it can be potentially supported by the LCM without any extra new hardware such as dispenser and advanced camera sensor which might require careful calibration [18, 19] at both ends. We herein present polarization-based QAM (PQAM), a new advanced modulation scheme that constructs the orthogonal basis of two (P)AM channels in the polarization domain.

4.2.1 *Orthogonal Basis in Polarization Domain*

In traditional QAM, the two orthogonal carrier waves use amplitude modulation, which corresponds to PAM in our LCM pixels setting. To modulate a specific amplitude, we charge ρ percentage of the LCM pixel and leave the remaining uncharged. As illustrated in Fig. 6, in the flicker-free setting where the front polarizer of LCD is detached for LCM-based polarized light transmission, we have two LCMs with size ratio of 1:2, the back polarizer has a polarization angle θ_t *relative to the vertical direction*, and the retroreflected light from the LCM pixels being charged or discharged has θ_t and $\theta_t + 90°$ (relative to the vertical direction) respectively when $\rho = 33\%$. Note that we assume a continuous ρ for generality, but in reality it takes only $\sqrt{P}$ discrete values for PQAM modulation by combining $\log_2 P$ binary weighted pixels in our prototype implementation.

According to Malus's law, the intensity when polarized light passes through another polarizer is: $I = I_0 \cos^2(\Delta\theta)$, where I_0 is the original intensity, and $\Delta\theta$ is the difference between the polarization angles of incident light and the polarizer. For the receiver whose polarization angle is θ_r, the received light intensity is:

$$\begin{aligned} I &= \rho \cos^2(\theta_t - \theta_r) I_0 + (1-\rho)\cos^2(\theta_t + 90° - \theta_r) I_0 \\ &= \rho \cos 2(\theta_t - \theta_r) I_0 + \sin^2(\theta_t - \theta_r) I_0, \end{aligned}$$

in which only the $\rho \cos 2(\theta_t - \theta_r)$ item or ρ is a variable corresponding the polarization distribution. Hence, the resulting channel coefficient regarding polarization is:

$$h_{tr} = \cos 2(\theta_t - \theta_r) = \begin{pmatrix} \cos 2\theta_t & \sin 2\theta_t \end{pmatrix} \begin{pmatrix} \cos 2\theta_r \\ \sin 2\theta_r \end{pmatrix}.$$

The above factorization indicates that we can consider the polarizers at the transmitter and receiver separately. Furthermore, we found that a pair of transmitters with a relative polarization angle of 45° forms an *orthogonal* basis of a 2D signal space with

$$\begin{pmatrix} \cos 2\theta_t & \sin 2\theta_t \end{pmatrix} \begin{pmatrix} \cos 2(\theta_t + 45°) \\ \sin 2(\theta_t + 45°) \end{pmatrix} = 0,$$

and this property of orthogonality also holds for a pair of receivers with relative polarization angle of 45°.

4.2.2 *From PAM to PQAM*

With the orthogonality analyzed above, we now describe the design of PQAM scheme as following: we divide the LCM pixels into two groups with relative polarization angle of 45°, called I-LCM and Q-LCM respectively, where each group forms a multi-level PAM modulator. A central controller is used to transmit data points (ρ_1, ρ_2) in the constellation plane, by charging ρ_1 part of I-LCM and ρ_2 part of Q-LCM, leaving the remaining uncharged. A concrete example of 4-PQAM is shown in Fig. 7.

The PQAM design is robust to the cases when the two ends are not aligned in terms of polarization angle, especially when in comparison to PDM[3]. The two receivers form an orthogonal basis as the transmitter does – if these two orthogonal bases at the transmitter

[3]In the example of two tx-rx pairs with polarization angle perpendicular to each other, a angular misalignment of $\Delta\theta$ can not only have the received light intensity attenuated to $I_0 \cos^2(\Delta\theta)$, but also introduce interference of $I_0 \sin^2(\Delta\theta)$ to the other channel.

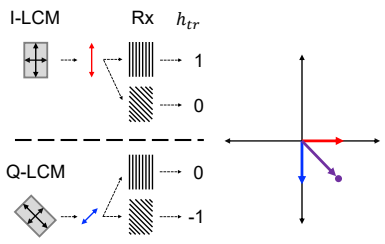

(a) The Symbol of '10'.

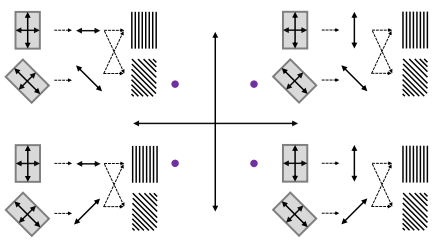

(b) Constellation diagram.

Figure 7: Illustration of 4-PQAM.

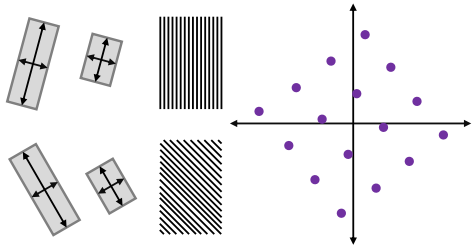

Figure 8: Rotated constellation with angular misalignment on two ends for 16-PQAM.

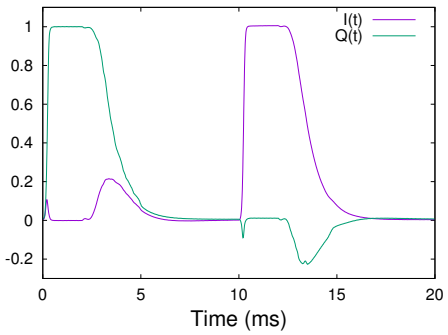

Figure 9: I/Q-LCM pulse responses.

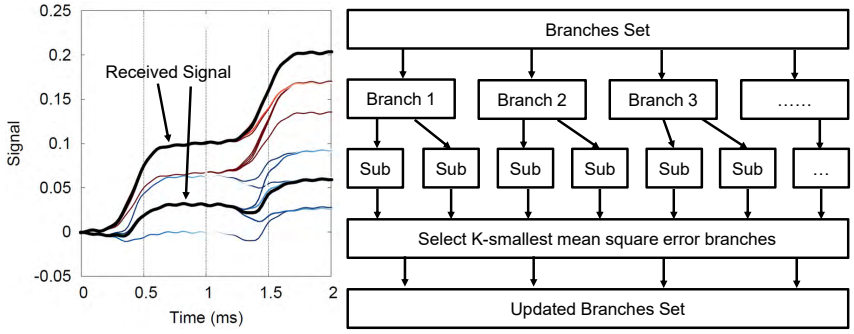

Figure 10: Workflow of Decision-feedback Equalizer with $K = 16$.

and receiver side has a deviation due to (physical) angular misalignment, it could be corrected by an orthogonal transformation, *i.e.,* a rotation in constellation plane, as illustrated in Fig. 8. This is why our PQAM is rotation-tolerant: a physical rotation of $\Delta\theta$ results in a $2\Delta\theta$ rotation in the constellation plane, and such rotation can be corrected by employing the solution in conventional QAM for dealing with a carrier phase offset. We will present an algorithm in preamble matching to correct this rotation in §4.3.1.

4.2.3 *Work with DSM Together*

The design of PQAM can be naturally integrated with DSM – by extending each DSM symbol to a multi-level PAM signal onto the in-phase (I) and quadrature (Q) in the P-order PQAM plane, one can boost the data rate up to: $L \times \log P$. For instance, an 8-order DSM and 16-order PQAM modulator is able to send as much as $8 \times \log 16 = 32$ bits in DSM symbol duration W.

While it sounds promising, combining DSM and PQAM poses several challenges in demodulation. The analysis of PQAM assumes a stable state of LCM, whereas in DSM every pulse is always either charging or discharging. However, transition state produces cross-channel interference as the polarity changes in theory. Interestingly, we find that the two pulses from I-LCM and Q-LCM satisfy $p_{\mathrm{I}}(t) = \sqrt{-1}p_{\mathrm{Q}}(t)$, as shown in Fig. 9, which means two synchronized pulses from both channels are *orthogonal at any time instant* and still can be transmitted together. Indeed, such orthogonality only holds for simultaneous, not succeeding pulses, *i.e.,* $\mathrm{Re}\int p_{\mathrm{I}}(t)p^*_{\mathrm{Q}}(t+kT)\mathrm{d}t = 0 \implies k = 0$ or $|k| \geq L$. Therefore, symbols from both channels must be considered together for ISI cancellation when $0 < |k| < L$. In the following demodulation process, we will continue using this notation of complex-valued pulse/waveform and aggregate the impact from both channels and each PAM modulator.

4.3 Receiver Design

We present how to design the preamble for PQAM rotation correction, a equalizer for DSM ISI elimination in demodulation with a channel training process dedicated for handling sub-channel heterogeneity from different LCM.

4.3.1 *Rotation Correction with Preamble Reference*

The preamble design of RetroTurbo should not only ensure its packet detection and frame alignment duty, but also the PQAM rotation correction unique to our proposal. In order to provide a sample-level timing precision, our detection directly looks for a *reference* waveform recorded offline under sufficiently high SNR. We denote this preamble reference of k samples as $Y[\tau]$ and received signals as $X[t]$. We assume a similarity function $D : \mathbb{C}^k \times \mathbb{C}^k \to [0, \infty)$, and the starting time t_0 of a packet should minimize $D(X[t_0, t_0 + k - 1], Y)$. We adopt a linear regression approach that models the rotation as well as amplitude and offset:

$$D(X, Y) = \arg\min_{a,b,c\in\mathbb{C}} \left\| Y - \left(aX + bX^* + c\right)\right\|^2,$$

where the complex coefficient a models rotation and scaling, c denotes DC offset, and the complex conjugate term bX^* is for I/Q imbalance in practice[4]. If a preamble is detected, the estimated coefficients a, b, c will be multiplied onto succeeding signal before demodulation. Note that the preamble reference is collected and calibrated to be rotation-free, and these coefficients that best match the received signal will be used to cancel the rotation and scaling for the rest of the packet.

4.3.2 *Demodulation with Decision-feedback Equalizer*

Given that DSM essentially results in an ISI channel (§4.1.2), our first goal is to design an equalizer that removes interference from previous symbols to successfully recover the current symbol. Since traditional linear equalizer is not able to equalize the nonlinearity of LCM, we choose to leverage decision-feedback equalizer (DFE) – when one decision of the current symbol is first made, we emulate its expected received waveform based on the knowledge of interference pattern and subtract it from succeeding received signal.

Next we decide the bits for output and feedback after previous ISI removed. The output of equalizer is a clean prefix waveform (*i.e.,* rising edge of a LCM pulse response), so it needs to be converted to a value before thresholding for decision. We use a least-squares criterion by a linear regression to decide a n-th PQAM symbol:

$$s_n = \arg\min_{s\in\mathbb{C}} \int_{nT}^{(n+1)T} |e_n(t) - sp(t - nT)|^2 \,\mathrm{d}t,$$

where $e_n(t) = r(t) - \sum_{m<n} I_m p(t - mT)$ is the nth equalizer output, and $p(t)$ is the pulse response of PQAM transmitters. Finally this complex coefficient s is a canonical QAM symbol and ready for decision. Note that DFE has suboptimal BER performance compared to maximum likelihood sequence estimator (MLSE) because of two reasons: i) it decides s_n according to the $[0, T)$ segment of the pulse $p(t)$ instead of full nonzero length $[0, W)$, and ii) it suffers

[4]Here we correct the signal's DC offset at the receiver side, while the transmitter's DC stress should be avoided with appropriate data scrambler applied.

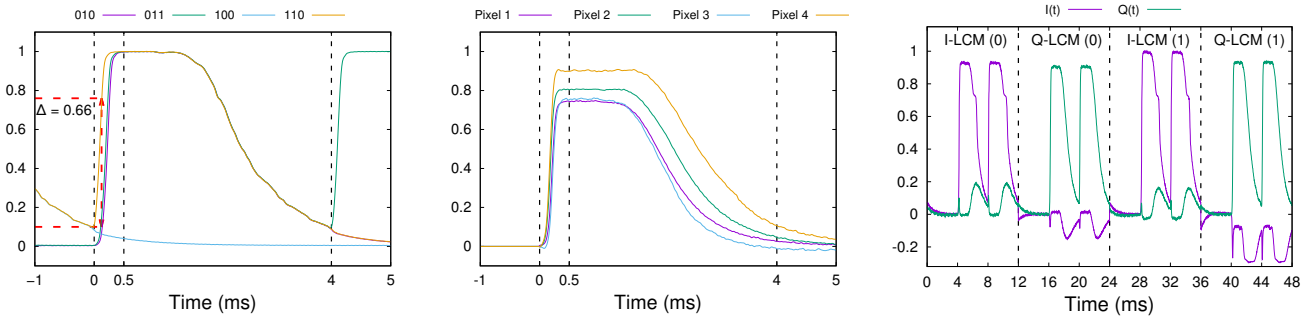

(a) Different previous bits. **(b) Different locations.**

Figure 11: Eye-diagram example of heterogeneous LCM pulse response.

Figure 12: Example reference waveforms of $r(s_1)..r(s_4)$ for one-time offline training.

from error propagation, *i.e.,* the first wrong symbol causes wrong equalizer output, which may lead to another symbol error. However, MLSE may suffer from high computation cost, which might lead to computational infeasibility for embedded real-time operation. Therefore, a suboptimal algorithm is preferred to balance between demodulating latency and BER performance.

The optimization strategy we choose is to store multiple branches for least square searching, *i.e.,* a set of K-least square equalizer output is stored as possible solutions. By merging the last L symbols in the set and $K = P^L$, it is exactly the Viterbi detector that is optimal however impractical with large P and L. With an appropriate K value, our equalizer can achieve both reasonable BER performance and practical demodulation latency. As shown in Fig. 10, a group of $K = 16$ possible solutions are stored and searched for the next PQAM symbol within T time slot, then after each round those branches with smaller mean square error are kept while others are rejected. This proves to be near optimal with DSM design that makes the signal highly distinguishable within the first T time slot, as to be evaluated later (Fig. 17a).

4.3.3 *Combating LCM Heterogeneity with Channel Training*

The implicit assumption of a uniform pulse response $p(t)$ over time and different LCM is invalidated by excessive demodulating errors in our experiments, because of the following two reasons: first, the pulse shape suffers from tail effect under small τ_0, so that it's not solely decided by current bit but also depends on the previous ones. As shown in Fig. 11a, the "010" pulse has a longer delay before ramping up than "110" pulse. The resulting system error is actually non-trivial within the first $T = 0.5$ ms interval; second, across multiple LCMs for DSM, the pulses vary in amplitude (Fig. 11b), possibly due to manufacturing error between LCMs, uneven illumination from different angle and distance, and angular errors of LCM's polarizer attachment. This will result in a scaled constellation and consequently symbols misidentified as nearby ones. Moreover, such temporal and/or spatial errors will accumulate when we equalize ISI using incorrect pulse responses.

To tackle these practical challenges, our key idea is to use different reference pulse for each LCM sub-channel to perform equalization and symbol regression. Therefore, the task of channel training is to estimate the reference pulse in each sub-channel per packet as the matched filter or template for demodulation, with reasonable accuracy but also avoiding overfitting to degrade the noise tolerance of the receiver.

For the property of tail effect, we employ a fingerprint-based model with finite-length memory, where we record multiple pulses from LCM transmitters and classify them according to V previous bits in addition to the current bit. A larger V will reduce bit error rate at cost of higher training time overhead. For final demodulation, this model incorporates naturally with the DFE scheme, where the i-th decided bit is used not only to equalize interference from other LCMs (*i.e.,* bit $i+1, i+2, ..., i+L-1$) but also select the correct reference pulse for this LCM (*i.e.,* bit $i, i+L..., i+(V-1)L$).

To mitigate the impact of LCM pulse diversity from different locations and different pixels, it is essential to balance reference precision and noise tolerance. One extreme case is to support no diversity at all but use virtually noiseless reference pulse, which is recorded offline and averaged from more than thousands of samples. The other extreme is to sample the reference pulse within the packet to best support diversity, which will however lead to a huge per-packet overhead (*i.e.,* at least several seconds) in order to achieve sufficiently low noise level (after averaging them out). This problem reduces to how to represent more effectively with as less degree of freedom as possible, and when confined to a linear model and MSE cost function, reveals itself as truncated (sorted by decreasing eigenvalue) Karhunen-Loève expansion because it does minimize squared error of all possible truncated linear approximations.

This theoretical perspective illuminates our two-fold approach of channel training: An offline training to extract a few invariant bases by examining multiple pulses taken from different locations of good SNR, and a per-packet online training to solve only the coefficients associated with these bases. Mathematically, let $r(x, v)[1..m]$ be a segment of pulse waveform of length $m = Wf_s$ with ADC sample rate f_s, which is a function of the spatial parameter x and temporal trace-parameter v. We first define $r(x)$ of $2^V m$ samples, a *union set* of $r(x, v)$ over all possible values of v[5], then concatenate and transpose it to a column vector. $r(x)$ as a complete behavior model for one LCM at the specific orientation is both the basic unit of offline training and final output of online training.

For offline training, $r(x)$ are collected at n different orientations $x_1 \dots x_n$ and arrange them in $(2^V m)$-by-n matrix:

$$E = [r(x_1) \dots r(x_n)]$$

[5] v is first enumerated by a maximum-length sequence – taking $(2^V - 1)W = 12$ ms to complete (Fig. 12), then padded an all-zero waveform

By calculating the SVD truncated to rank S:

$$E = U\Sigma V^H + \varepsilon,$$

we extract the S column vectors of matrix U as our reference bases. Then the online training is solving S coefficients of the truncated bases for each one of the $2L$[6] LCM modules. In each packet, a linear-independent pattern set of $2L$ bits is assigned to each one of $2L$ transmitters sent simultaneously. The receiver then finds the least-square solution of $2SL$ unknowns from received signal accordingly.

4.4 Rate-Adaptive MAC Protocol

The PHY layer design above opens up the opportunity of multi-rate adaptation. Since different modulation scheme (and the order) has different demodulation SNR threshold (to be analyzed in §5), we can develop a rate-adaptive MAC protocol to assign the "optimal" bit rate (and coding rate) to each RetroTurbo tag based on the uplink SNR for performance and reliability enhancement. Thanks to the intrinsic ultra-narrow directionality property of retroreflective uplink communication, its path loss model has a more deterministic relationship to the distance than RF-based technology because of less multipath effect and interference.

We design a thin MAC layer to manage the reader and tags in the master-slave mode based on a simple TDMA protocol. We develop a tag discovery protocol similar to that used in RFID system to retrieve all the tag ID information, and piggyback the suggested bit rate and coding rate in the downlink message based on the SNR measurement and a database profiled with real world experimental data. The MAC will trigger retransmission when CRC check fails.

We note that a full-fledged MAC design shall also incorporate more functions such as multi-reader coordination and uplink collision avoidance, which we leave for future work.

5 MODULATION SCHEME ANALYSIS

The joint design of DSM and PQAM utilizes the unique temporal and polarization attributes of LCM. However, from the analytical perspective, there are three questions need to be answered in order to maximize the performance of RetroTurbo and apply them to other similar communication systems, especially those with nonlinear modulator: *i) How to judge whether one modulation scheme is better than another, at what extent? ii) How to emulate nonlinear LCM accurately with an error bound for analysis? iii) What is the optimal parameters given the specific nonlinear modulator and data rate target?* We answer these questions in the rest of this section.

5.1 Performance Index

With N individual modulators (*e.g.,* LCM pixels in our case), a modulation scheme is abstracted as a mapping function between k bits data x and a binary matrix of $N \times M$ elements called code matrix A, where M is the amount of discrete time slots. There is a mapping function F between code matrix and a series of signal over time $[0, t_0 + k/R]$, where R is data rate and t_0 is a constant duration of limited tail effect. In AWGN channel, the received signal $r(t) = F(A)(t) + n(t)$ given noise signal $n(t)$. The Euclidean distance of two code matrix A and B is $|A, B|$ defined below, where the minimum distance $D = \min\left\{|A, B| \middle| A \neq B\right\}$ of a modulation scheme determines the demodulation threshold $\mathtt{SNR}_{\mathtt{th}} = 10\log_{10} D(dB)$:

$$\underset{(N\times M)}{A} = \begin{pmatrix} 1 & \cdots & 1 & 1 & 0 \\ 0 & \cdots & 0 & 1 & 1 \\ \vdots & & \vdots & \vdots & \vdots \\ 1 & \cdots & 1 & 0 & 1 \\ 0 & \cdots & 0 & 0 & 1 \\ 1 & \cdots & 0 & 1 & 0 \end{pmatrix}, \quad \begin{aligned} F(A) &= f(t), t \in [0, t_0 + k/R] \\ |A, B| &= \int_0^{t_0+k/R} |F(A)(t) - F(B)(t)|^2 dt \end{aligned}$$

Suppose all the time slots are equally spaced and each time slot lasts $\Delta t = \frac{k}{RM}$. For an ideal modulator with infinite bandwidth $F(A)(t) = A_{1,\lfloor \frac{RM}{k} \times t \rfloor}$ with single pixel $N = 1$ as an example, the traditional OOK modulation has $M = k$, $A_{1j} = x_j$ and $D = \frac{k}{RM} = \frac{1}{2R}$ (*i.e.,* minimum distance happens at single bit inverse). For the ideal modulator above, it can be proved that OOK is one of the best modulation schemes in the measure of D. However, it is hard to model and analyze nonlinear modulators such as LCM. Approximation techniques can be used to find near optimal modulation strategies.

In short, modulation scheme with a larger D indicates it is a one with better performance index because it can tolerate higher noise level and thus has a lower demodulation threshold. In other words, a small value of D means that two distinct data sequences result in very similar received waveforms which are indistinguishable even under low noise level. We would also like to note that D does not map to BER directly because coding scheme can be always incorporated to reduce bit errors, *e.g.,* Gray code in PAM.

5.2 LCM Emulation

LCM has an infinite and nonlinear pulse response based on its physical model of electric, elastic and viscous forces [16], which poses challenges for mathematical modeling. However, it is still feasible to use finite sequence to approximate and emulate the behavior of LCM with limited error bound by limiting the tail effect to the recent V bits. We leverage V^{th}-order M-sequence (MLS) with time slot of $\Delta t = 0.5$ ms to collect reference $R_{[b_1 b_2 \cdots b_V]}(t)$ of this nonlinear modulator where $[b_1 b_2 \cdots b_V]$ is the previous V bits. This reference is then used to estimate the error bound of shorter sequences, with maximum and average relative errors shown in Tab. 2. Higher V emulates response of LCM more accurately, which however requires exponentially more time to collect. For instance, $V = 4$ only takes the previous 4 bits (2 ms) into account, which is even smaller than discharging phase, and consequently it cannot accurately emulates the response of LCM. We use $V = 16$ (8 ms) to balance the emulation error and data collection overhead for analyzing modulation scheme performance.

MLS Order (V)	4	6	8	10	12	14	16
Maximum	59%	31%	21%	13%	7.3%	3.2%	0.7%
Average	15%	4.1%	1.2%	0.4%	0.2%	0.2%	0.1%

Table 2: Relative error $\sqrt{\sum_{i=1}^{N}(f[i] - f_{V=17}[i])^2/N}$.

Since each pixel is independent and satisfies the approximate model above, the i-th pixel with signal amplitude of G_i has a response only related to previous V bits. The signal of each pixel is

[6]Each polarization channel has L DSM transmitters. We assume that each PAM transmitter is small and manufactured identical enough so that the reference is exactly proportional to each pixel area.

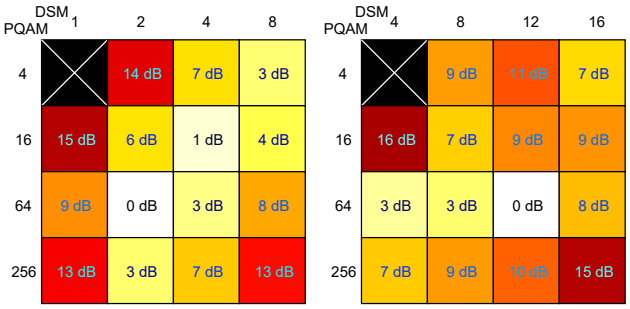

(a) 8 Kbps **(b) 32 Kbps**

Figure 13: Relative demodulation threshold.

superimposed linearly, so the overall signal at any given time t is

$$F(A) = \sum_{i=1}^{N} G_i \times R_{[A_{i,j-V+1},\cdots,A_{i,j}]}(t - j\Delta t), j = \lceil \frac{t}{\Delta t} \rceil$$

5.3 Optimal Parameters

With the emulation method above and a target rate R, one can search for the optimal parameters of DSM and PQAM, *i.e.,* DSM order, PQAM order. The relative demodulation threshold (Fig. 13) shows that a proper combination of DSM and PQAM together reaches the best performance. The performance indexes D and demodulation thresholds of optimal paramters are shown in Tab. 3.

Data rate (Kbps)	1	4	8	12	16
D	8.7	9.0e−2	1.5e−2	7.8e−3	4.0e−3
Threshold	0 dB	20 dB	28 dB	31 dB	33 dB

Table 3: Demodulation threshold of optimal parameters.

We leverage the optimal parameters derived here (also validated by real-world experiments) for choosing DSM and PQAM order to carry out experimental evaluation. The emulation method of nonlinear LCM is used in §7.3 for trace-driven emulation.

6 IMPLEMENTATION

Our prototype includes a pair of MCU-controlled hardware tag and reader that perform basic functionalities of timing, controlling individual pixels and receiving ADC samples (Fig. 14), and auxiliary computers on both ends to run (de-)modulation algorithms.

Reader. It incorporates the switching carrier and passband receiver design [9] in order to avoid baseband ambient light variations. To support the corresponding 2 PQAMa channels, we duplicate its Photodiode-Amplifier-ADC chain and lay out them in 3 PCBs – a pair of frontend PCBs, each consisting of two BPW34 photodiodes and a OPA2356 1st-stage LNA, and a backend PCB for two VCA821 amplifiers and STM32H750 MCU. The two frontend PCBs are encapsulated in 3D-printed cases where polarizers stick upon, shielded by cooper foil for EMC and glued to a 3D-printed octagonal frame that pinpoints a 45° angle (§4.2.1) atop the flashlight, as shown in Fig. 14a. The backend MCU converts two analog channels with its integrated ADCs, and performs basic processing, namely gain control, down-conversion and decimation before streaming to host computer with its embedded USB port. Note that we equip reader with two pairs of 2-photodiode for 0° and 45° PQAM signal reception – each pair further adopts the polarization-based differential reception (PDR) design [11] with two front polarizers orthogonal to each other for SNR improvement purpose.

Tag. It is built as an array of 4 LCMs covering a sheet of 3M 8912 retroreflective fabric with total area of 66 cm^2. The LCMs are customized in a way that each one contains 4 groups of pixels with area ratio 8:4:2:1 to realize ASK up to 16 levels (256-QAM), as shown in Fig. 14b. The 4 LCMs are equipped with either 0° or 45° back polarizer, forming 2 I-LCMs and 2 Q-LCMs respectively. To avoid a mess of wires to control these $4 \times 4 \times 4 = 64$ independent pixels, we use SN74LV595 shift registers to control the pixels; the registers are daisy-chained on an SPI bus. An STM32L432 MCU modulates data and sends them through the SPI bus.

7 EVALUATION

7.1 Experimental Setup

We evaluate RetroTurbo primarily using real world experiments based on our prototype, as shown in Fig. 15. The reader is powered with 4 W and set FOV to ±10°. Unless explicitly stated, the interrelated system parameters are set to default, including the data rate of 8 Kbps, no roll and yaw angular misalignment, and ambient light condition of typical illuminated office at night (*i.e.,* around 200 lux). For each data point, the tag sends 30 packets of 128 bytes (~30K bits), and we use bit error rate (BER) as the metric for uplink evaluation. In general, we assume a PHY link can be regarded as reliable

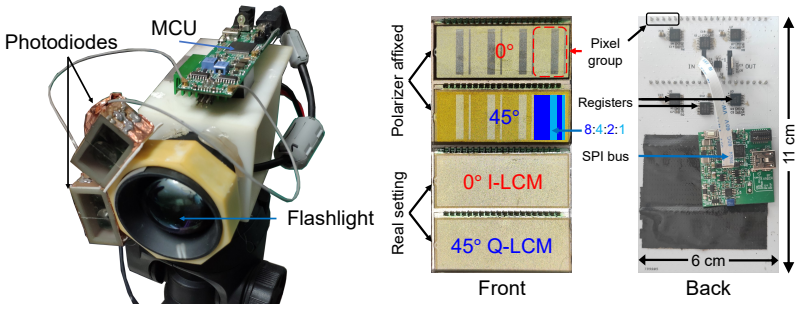

(a) Reader. **(b) Tag.**

Figure 14: RetroTurbo prototype.

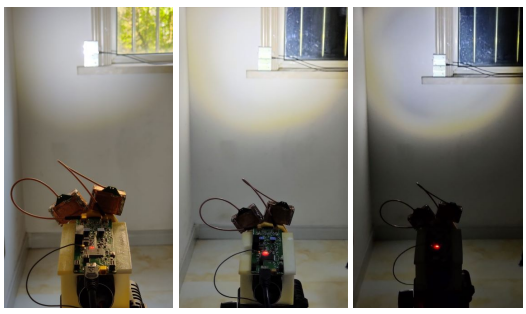

(a) Day (1000 lux) (b) Night (200 lux) (c) Dark (20 lux)

Figure 15: Experimental setup.

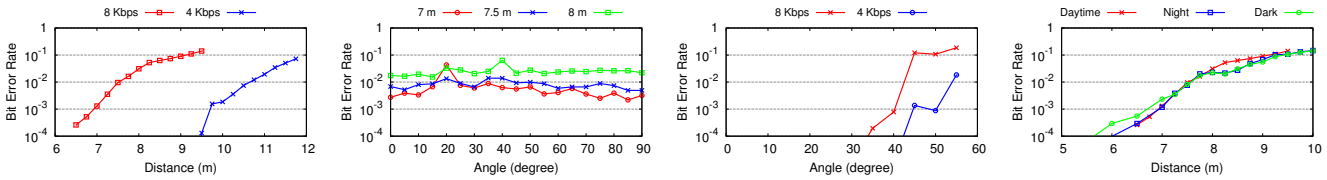

(a) Communication range. **(b) Roll angular misalignment.** **(c) Yaw angular misalignment.** **(d) Ambient light condition.**

Figure 16: BER basic results.

(provided error correction coding and sporadic retransmission are applied to eliminate errors) if its BER is less than 1%.

7.2 Experimental Evaluation

7.2.1 *Bit Error Rate Results*

Uplink Rate. We first measure the impact of data rate by the Line-of-Sight communication distance between tag and reader. Fig. 16a shows a working range of 7.5 m is achievable for an 8 Kbps link, and the range increases to 10.5 m for 4 Kbps. We believe such communication ranges are adequate for most indoor IoT applications.

Roll Angular Misalignment. Benefiting from the PQAM design, RetroTurbo is tolerant to arbitrary roll angles theoretically. We evaluate the BER from different roll angles as shown in Fig. 16b, and observe that the influence of roll angular misalignment is almost negligible, for both inside and outside range of 7.5 m.

Yaw Angular Misalignment. In real-world deployments, it is very likely that a tag may not face the reader squarely, *i.e.,* the tag's surface is not perpendicular to the beam of the reader. This might lead to a decline in SNR from reduced projection area, or a received symbol deviation from the reference symbol. As shown in Fig. 16c, our channel training design makes RetroTurbo tolerate at least ±40° of yaw angular misalignment by calibrating the symbol deviation. The preamble detection and channel training will likely to fail beyond ±55° of yaw angular misalignment.

Ambient Light Condition. Ambient light can introduce background noise and potentially degrade VLC link performance. We carry out experiments in indoor settings under different ambient light conditions. As shown in Fig. 16d, RetroTurbo behaves consistently regardless of the illumination level of ambient light. This is because *i*) the indoor light intensity from ambient light is already attenuated to the extent not to saturate the light sensor, which leave enough (SNR) headroom for RetroTurbo to carry information bits; *ii*) the ambient light will be converted to a DC signal and filtered out by our bandpass filter, unlike the RetroTurbo signal operating at a high carrier frequency of 455 KHz. The results demonstrate that RetroTurbo is adaptable to most typical indoor environments.

Test case	No human	1 person walks 10 cm off LoS	1 person walks behind the Tag	1 person works 5 cm off LoS	3 people walk around LoS
BER (%)	0.25	0.25	0.11	0.29	0.17

Table 4: BER with ambient human mobility.

Ambient Human Mobility. Practical indoor environments typically involve ambient human mobility, which can reflect wireless signals, introduce multipath effect and degrade receiver performance. Unlike radio (backscatter) communication, the downlink directionality and uplink retroreflectivity brings the intrinsic advantage of minimal ambient reflection and scattering in RetroTurbo and VLBC in general. To verify that the BER performance of RetroTurbo is robust to ambient human mobility, we design five test cases incorporating human location, mobility level and number of people factors, and send 30 packets (same as other experiments) for comparative evaluation. As shown in Tab. 4, all the human mobility cases do not exhibit significant higher BER in comparison to the "no human mobility" baseline, and their BERs are all below 0.3%.

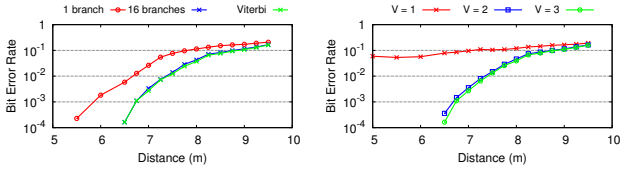

(a) Demodulation DFE branches. **(b) Channel Training.**

Figure 17: Microbenchmark results.

7.2.2 *Microbenchmark*

Decision-feedback Equalizer. Our DFE demodulator balances between computing latency and BER performance. As shown in Fig. 17a, while the naive single-branch DFE demodulator is much worse than optimal Viterbi demodulator, *i.e.,* about 0.7 m or 10% loss in working range, a 16-branches DFE demodulator has BER performance nearly close to the optimal one, introducing only 16 times more computational cost which supports real-time demodulation.

Channel Training. It focuses on how to select V to balance between BER performance and $O(2^V)$ training time. Fig. 17b shows that $V = 1$ has inferior performance even with sufficient SNR, which is depicted as a system error (Fig. 11a). The default experiment setup of $V = 2$ has subtle BER performance lost compared to $V = 3$ ones, while reduces 50% offline channel training time.

Latency. It comes from packet transmission, online channel training and demodulation. The preamble and online training consumes 50 ms and 80 ms respectively. We measure the packet of default setup in §7.1 whose packet transmission time is 258 ms for 8 Kbps and 386 ms for 4 Kbps, and channel training consumes 27 ms in average. Both 8 Kbps and 4 Kbps consumes 90 ms for demodulation with 16-branches DFE, which is less than payload length of 128 ms or 256 ms to support real-time pipelined demodulation. The demodulation time grows exponentially with DSM order while remains the same regardless of PQAM order. The overall latency for a 128-byte packet transmission is 375 ms and 503 ms respectively. More specifically, it takes 1.35 ms and 1.17 ms to transmit and receive a single RetroTurbo symbol under 4 Kbps and 8 Kbps respectively.

Power. We use Moonsoon [20] to measure the power consumption of RetroTurbo tag, which takes 0.8 mW in both 4 Kbps and 8 Kbps settings. This is because they share the same DSM symbol

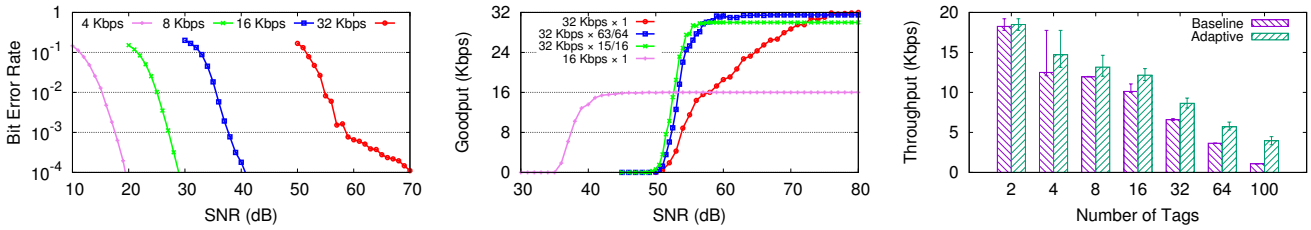

(a) High order modulation. **(b) Coding gain.** **(c) Rate adaptation.**

Figure 18: Emulation results.

length, and the power consumption on I-PCM and Q-QAM are equal. Higher data rate will not change DSM symbol length which is limited by inherent attribute of LCM, thus the energy consumption remains the same. The sub-mW property potentially facilitates battery-free operation with solar panel.

7.3 Emulation Results

We further complement with our experiments with a set of trace-driven emulation based on experimental data to evaluate RetroTurbo in the cases with more LCM pixels and tags.

Higher Order Modulation. The highest rate of 8 Kbps we achieved is primarily limited by the imperfect linearity in the photodiode and high noise floor from the imperfect receiver circuit implementation[7]. In order to push the highest order modulation and data rate limit that RetroTurbo can achieve, we separate the design from the implementation and choose to carry a emulation-based evaluation. Specifically, we collected the reference waveform of symbols, and generated the emulated waveform by superimposing different levels of additive white Gaussian noise upon the signal with different DSM and PQAM parameter setups. Fig. 18a shows the relationship between BER and SNR of different modulation orders. RetroTurbo achieves up to 32 Kbps under a 55 dB SNR restriction, corresponding to a communication range of 3.5 m. Note that a even higher rate is possible at the cost of even higher SNR, which is impractical in real world use cases. According to the analysis in §5.3, The optimal parameters selected for 1 Kbps has a demodulation threshold of 20 dB better than 4 Kbps in this case, meaning that demodulating 1 Kbps has a -5 dB SNR restriction at 1% BER.

Coding Gain. To better understand how the reliability of links benefits from error correction, we carry out a series of emulations with Reed-Solomon Code. Fig. 18b shows the goodput results with different error correction settings based on stop-and-wait retransmission mechanism. A 32 Kbps link with error correction has higher goodput than both 32 Kbps and 16 Kbps raw links in a SNR range of 22 dB, only at the cost of 1/64 of the max throughput when SNR is sufficiently high. On the other hand, a lower coding rate enables a wider working range of SNR at the cost of maximum goodput.

Rate Adaptation. The coding gain study above provides a mapping between SNR and the highest goodput as well as the corresponding bit rate and coding rate. We carry a MAC rate adaptation study in which a reader will assign different rate for each tag based on the SNR proportional to the distance between two ends. To approximate the indoor setting, the reader's FoV is adjusted to 50° but still powered with 4 W. The tags are randomly distributed with a distance from reader between 1 m and 4.3 m, corresponding to the 65 dB and 14 dB of SNR based on link budget model [9] validated and fitted with our experimental measurement. We use mean throughput from all the tags as the performance metric and run the test for 100 times. For baseline, all the tags are assigned the lowest bit rate for appropriate for the one with the lowest SNR. As shown in Fig. 18c, our rate adaptation achieves increasingly better performance than baseline as more tags are deployed, *e.g.*, the network rate gain is up to 1.2x with 4 tags and 3.7x with 100 tags. Note that the rate adaptation here is in the context of a number of networked tags – it still works for any single tag when its SNR changes in operation.

[7]Our tag design supports up to 16 Kbps data rate with 8-DSM and 256-PQAM.

7.4 Summary of Key Results

Our evaluation demonstrates that RetroTurbo prototype can operate a 8 Kbps VLBC link reliably within 7.5 m, robust to angular misalignment and ambient lighting conditions in indoor settings, and under sub-mW power budget. Beyond the implementation constraints, the RetroTurbo design pushes the rate limit to 32 Kbps and improves the aggregated throughput by up to 3.7x with link-aware rate adaptation in networked environment.

This work does not raise any ethical issues.

8 DISCUSSION

Photodiode versus Camera as Receiver. Demodulating the (DSM) signal in our system requires sub-ms time resolution, which is easy for photodiode but not for COTS camera. In addition, a camera is designed to perform average exposure for the full view and thus fails to take advantage of the retroreflectivity for long-range communication. Nevertheless, our design can serve as a new element to customize the camera design for special requirement.

Efficient Multiple Access. The DSM and PQAM designs are designed for single device rate boosting. To make it more general, a reader can potentially coordinate the transmission state on LC pixels distributed in multiple tag devices for efficient parallel decoding from their concurrent transmission. With multiple photodiodes placed strategically from optical channel diversity perspective, one can further develop MIMO system in the context of VLBC.

Mobility Support. Our channel training procedure is designed to make the demodulation procedure robust to the angular misalignment and LC heterogeneity in static, which might not hold when either end is in mobility, especially when packet is relatively long. One possible solution would be inserting multiple synchronization frames based on the mobility level and packet length to perform dynamic channel equalization.

9 RELATED WORK

Visible Light Backscatter Communication. By employing LCD(s) as an optical modulator, the series of work realized a retroreflecting link over the incoming light (carrier) from existing lighting infrastructure using OOK [9, 11, 21] and PAM [10] with a single and multiple LCD pixels respectively. The work [22, 23] embeds barcodes onto the surface of mobile objects and realizes passive communication by reading the optical pulse reflection from ambient light. Our work boosts the data rate by 8 times and 32 times over the status-quo in experimental and emulation results.

Polarized Light Communication. The ability of polarization manipulation in the LCD design [24] opens a new direction in building a polarized VLC system. PIXEL [18] leveraged dispersors to translate (relative) polarization direction into color and devise Binary Color Shift Keying modulation with fine dispersion tuning to maximize the intensity difference of the two states in all receiving orientations. POLI [25] combines three light sources of different polarization directions with a dispersor and map their transmitting intensity to the received RGB values to realize polarization intensity modulation. The work [19] presents a light polarization pattern realized by a polarizer and birefringent film for grid-level positioning and a dual-sensor design that examines the differential color values of two collocated color sensors to remove ambient light noise. PolarTag [26] uses polarizer and birefringent tape to build a passive visual tag with invisible data to human eyes, which has higher robustness and comparable data capacity than QR code. Our design shares the same philosophy of using polarization(-based modulation) but focuses on link aggregation without using color information (via dispersor) in retroreflective communication.

Polarization Division Multiplexing. The idea of utilizing and inverse-multiplexing independent polarization channels for link (bandwidth) aggregation has been explored in [16, 27, 28]. Recent simulation work [13] demonstrates the upper bound of PDM is 3 channels. PQAM is essentially a new PDM design and is advantageous in supporting arbitrary rotatory misalignment between the two ends. Note that our PQAM design is different from polarization QAM (POL-QAM) [29], which models a combination of PDM and conventional phase-based QAM in fiber-optics communication.

10 CONCLUSION

State-of-the-art practical visible light backscatter communication system only offers a sub-Kbps rate limited by LCD's slow response. In this paper, we revisit the material and optical properties of the LCM and propose two novel modulation schemes that fully exploit its asymmetric response and polarization manipulation capability to push the rate limit by an order with an array of LCM pixels. We believe our design can be generalized to and benefit other communication cases holding these optical properties.

ACKNOWLEDGMENTS

We are grateful to the anonymous shepherd and reviewers for their constructive and insightful critique, which have helped us greatly improve this paper. This work is supported in part by National Key Research and Development Plan, China (Grant No. 2016YFB1001200), National Natural Science Foundation of China (Grant No. 61802007), 111 Project (Grant No. B14025) and Microsoft Research Asia. Chenren Xu is the corresponding author.

REFERENCES

[1] Bryce Kellogg, Aaron Parks, Shyamnath Gollakota, Joshua R Smith, and David Wetherall. Wi-fi backscatter: internet connectivity for rf-powered devices. In *ACM SIGCOMM*, 2015.
[2] Dinesh Bharadia, Kiran Raj Joshi, Manikanta Kotaru, and Sachin Katti. Backfi: High throughput wifi backscatter. In *ACM SIGCOMM*, 2015.
[3] Bryce Kellogg, Vamsi Talla, Shyamnath Gollakota, and Joshua R Smith. Passive wi-fi: bringing low power to wi-fi transmissions. In *USENIX NSDI*, 2016.
[4] Pengyu Zhang, Colleen Josephson, Dinesh Bharadia, and Sachin Katti. Freerider: Backscatter communication using commodity radios. In *ACM CoNEXT*, 2017.
[5] Anran Wang, Vikram Iyer, Vamsi Talla, Joshua R Smith, and Shyamnath Gollakota. Fm backscatter: Enabling connected cities and smart fabrics. In *USENIX NSDI*, 2017.
[6] Vamsi Talla, Mehrdad Hessar, Bryce Kellogg, Ali Najafi, Joshua R. Smith, and Shyamnath Gollakota. Lora backscatter: Enabling the vision of ubiquitous connectivity. In *ACM UbiComp*, 2017.
[7] Yao Peng, Longfei Shangguan, Yue Hu, Yujie Qian, Xianshang Lin, Xiaojiang Chen, Dingyi Fang, and Kyle Jamieson. Plora: a passive long-range data network from ambient lora transmissions. In *ACM SIGCOMM*, 2018.
[8] Peter A Iannucci, Ravi Netravali, Ameesh K Goyal, and Hari Balakrishnan. Room-area networks. In *ACM HotNets*, 2015.
[9] Xieyang Xu, Yang Shen, Junrui Yang, Chenren Xu, Guobin Shen, Guojun Chen, and Yunzhe Ni. Passivevlc: Enabling practical visible light backscatter communication for battery-free iot applications. In *ACM MobiCom*, 2017.
[10] Sihua Shao, Abdallah Khreishah, and Hany Elgala. Pixelated vlc-backscattering for self-charging indoor iot devices. *IEEE Photonics Technology Letters*, 29(2), 2017.
[11] Purui Wang, Lilei Feng, Guojun Chen, Chenren Xu, Yue Wu, Kenuo Xu, Guobin Shen, Kuntai Du, Gang Huang, and Xuanzhe Liu. Renovating road signs for infrastructure-to-vehicle networking: a visible light backscatter communication and networking approach. In *ACM MobiCom*, 2020.
[12] Ander Galisteo, Diego Juara, Qing Wang, and Domenico Giustiniano. Openvlc1.2: Achieving higher throughput in low-end visible light communication networks. In *IEEE/IFIP WONS*, 2018.
[13] Darko Ivanovich, Samuel B Powell, Viktor Gruev, and Roger D Chamberlain. Polarization division multiplexing for optical data communications. In *Optical Interconnects XVIII*, 2018.
[14] Volodymyr Borshch, Sergij V Shiyanovskii, and Oleg D Lavrentovich. Nanosecond electro-optic switching of a liquid crystal. *Physical review letters*, 111(10), 2013.
[15] AK Srivastava, Wei Hu, VG Chigrinov, AD Kiselev, and Yan-Qing Lu. Fast switchable grating based on orthogonal photo alignments of ferroelectric liquid crystals. *Applied Physics Letters*, 101(3), 2012.
[16] Jong-Man Kim, Seung-Hyuck Lee, Dong-Hwan Jeon, and Seung-Woo Lee. Physical model of pixels in twisted nematic active-matrix liquid crystal displays. *IEEE Transactions on Electron Devices*, 62(10), 2015.
[17] Peter Kabal and Subbarayan Pasupathy. Partial-response signaling. *IEEE Transactions on Communications*, 23(9), 1975.
[18] Zhice Yang, Zeyu Wang, Jiansong Zhang, Chenyu Huang, and Qian Zhang. Wearables can afford: Light-weight indoor positioning with visible light. In *ACM MobiSys*, 2015.
[19] Zhao Tian, Yu-Lin Wei, Wei-Nin Chang, Xi Xiong, Changxi Zheng, Hsin-Mu Tsai, Kate Ching-Ju Lin, and Xia Zhou. Augmenting indoor inertial tracking with polarized light. In *ACM MobiSys*, 2018.
[20] Monsoon power monitor. http://www.msoon.com/LabEquipment/PowerMonitor.
[21] Jiangtao Li, Angli Liu, Guobin Shen, Liqun Li, Chao Sun, and Feng Zhao. Retro-vlc: Enabling battery-free duplex visible light communication for mobile and iot applications. In *ACM HotMobile*, 2015.
[22] Qing Wang, Marco Zuniga, and Domenico Giustiniano. Passive communication with ambient light. In *ACM CoNEXT*, 2016.
[23] Rens Bloom, Marco Zuniga, Qing Wang, and Domenico Giustiniano. Tweeting with sunlight: Encoding data on mobile objects. In *IEEE INFOCOM*, 2019.
[24] Pochi Yeh and Claire Gu. *Optics of liquid crystal displays*. John Wiley & Sons, 2010.
[25] Chun-Ling Chan, Hsin-Mu Tsai, and Kate Ching-Ju Lin. Poli: Long-range visible light communications using polarized light intensity modulation. In *ACM MobiSys*, 2017.
[26] Zhao Tian, Charles J Carver, Qijia Shao, Monika Roznere, Alberto Quattrini Li, and Xia Zhou. Polartag: Invisible data with light polarization. In *ACM HotMobile*, 2020.
[27] Paul M Hill, Robert Olshansky, and WK Burns. Optical polarization division multiplexing at 4 gb/s. *IEEE photonics technology letters*, 1992.
[28] Yuanquan Wang, Chao Yang, Yiguang Wang, and Nan Chi. Gigabit polarization division multiplexing in visible light communication. *Optics letters*, 2014.
[29] Henning Bulow. Polarization qam modulation (pol-qam) for coherent detection schemes. In *Optical Fiber Communication Conference*. Optical Society of America, 2009.